Nanoscale Advances

ROYAL SOCIETY OF CHEMISTRY

PAPER

View Article Online
View Journal | View Issue

Cite this: *Nanoscale Adv.*, 2022, **4**, 1639

Ultrafine platinum nanoparticles supported on N,S-codoped porous carbon nanofibers as efficient multifunctional materials for noticeable oxygen reduction reaction and water splitting performance†

Xiaohong Chen, [a] Kai Niu,[b] Zhiyong Xue, [a] Xundao Liu,*[c] Bogu Liu,[a] Bao Zhang,[a] Hong Zeng,[a] Wei Lv,[a] Yongming Zhang*[b] and Ying Wu*[a]

The design of highly active, stable and durable platinum-based electrocatalysts towards the oxygen reduction reaction (ORR), oxygen evolution reaction (OER), hydrogen evolution reaction (HER), and hydrogen adsorption has a high and urgent demand in fuel cells, water splitting and hydrogen storage. Herein, ultrafine platinum nanoparticles (Pt NPs) supported on N,S-codoped porous carbon nanofibers (Pt–N,S-pCNFs) hybrids were prepared through the electrospinning method coupled with hydrothermal and carbonation processes. The ultrafine Pt NPs are sufficiently dispersed and loaded on pCNFs and codoped with N and S, which can improve oxygen adsorption, afford more active sites, and greatly enhance electron mobility. The Pt–N,S-pCNFs hybrid achieves excellent activity and stability for ORR with ~70 mV positive shift of onset potential compared to the commercial Pt/C-20 wt% electrocatalyst. The long-term catalytic durability with 89.5% current retention after a 10 000 s test indicates its remarkable ORR behavior. Pt–N,S-pCNFs also exhibits excellent HER and OER performance, and can be used as an efficient catalyst for water splitting. In addition, Pt–N,S-pCNFs exhibits an excellent hydrogen storage capacity of 0.76 wt% at 20 °C and 10 MPa. This work provides novel design strategies for the development of multifunctional materials as high-performance ORR catalysts, water splitting electrocatalysts and hydrogen storage materials.

Received 7th January 2022
Accepted 11th February 2022

DOI: 10.1039/d2na00014h

rsc.li/nanoscale-advances

Introduction

Fuel cells, electrochemical water splitting and hydrogen storage have been identified as green and renewable energy conversion, production and storage systems, respectively, due to their significant large-scale applications, high efficiency, and low pollution or greenhouse gas emission.[1–6] The sluggish kinetics of catalysts in the oxygen reduction reaction (ORR), oxygen evolution reaction (OER) and hydrogen evolution reaction (HER) are known to govern their performance in energy utilization and power output.[7–14] Generally, platinum (Pt) on carbon materials has been widely used for ORR,[15–17] OER,[18–20] HER,[21–23] and hydrogen storage.[24–29] However, these catalysts require relatively large surface area, high electrical conductivity of carbon materials, and high loading density and uniform dispersion of platinum nanoparticles (NPs). To enhance the electrocatalytic activity and durability, carbon-supported materials can be doped by heteroatoms[30,31] such as nitrogen (N) or sulfur (S), which could effectively induce anchoring sites for the deposition of metal nanoparticles as well as afford more active sites[32–35] and electron mobility.[36–38] The electronic structure of Pt-based catalysts is modulated by the coordination of the nitrogen atoms doped on graphene sheets with the facial Pt atoms on the Pt NPs,[39] which can enhance the catalytic activity and durability.

Pt NPs uniformly dispersed on carbon materials are also significant for electronic reactions. Over the years, many studies have focused on methods to uniformly disperse Pt NPs. Pt NPs have been prepared by a polymer-coating method using nitrogen-containing polymers.[40–42] The surface of carbon materials evenly and strongly attached to polybenzimidazole through π–π interactions, indicating that the high-dispersibility Pt NPs were immobilized by nitrogen atoms to achieve better catalytic performance for ORR.[43–45] Pt NPs have also been prepared by $NaBH_4$ and ethylene glycol methods. Pt NPs in Pt/MnO_2-carbon

[a]*Institute of Advanced Materials, North China Electric Power University, Beijing. E-mail: yingwu2000@hotmail.com*

[b]*School of Chemistry and Chemical Engineering, Shanghai Jiao Tong University, No. 800 Dongchuan Rd., Minhang District, Shanghai 200240, China. E-mail: ymzsjtu@gmail.com*

[c]*School of Materials Science and Engineering, University of Jinan, Jinan, 250022, China. E-mail: mse_liuxundao@ujn.edu.cn*

† Electronic supplementary information (ESI) available. See DOI: 10.1039/d2na00014h

nanofibers were prepared using $NaBH_4$, and the resultant catalysts exhibit excellent electrochemical properties.[46] Pt–graphene hybrids were also synthesized *via* the thermolytic reduction of Pt(II) precursors on a carbon fiber substrate fabricated through the chemical oxidation and exfoliation of carbon fibers. The hybrids exhibit remarkable electrocatalytic activity during oxygen reduction.[47] In addition, carbon materials decorated with certain precious metals[48–51] can store a higher amount of hydrogen[52–55] compared to metal hydrides.[56–58] Graphene decorated with Pd and Pt has been proven to be the most promising hydrogen storage material due to its reasonable relationship of adsorption energies.[59] Although encouraging progress has been achieved, multifunctional materials for ORR, OER, HER and hydrogen storage still need more investigation.

Herein, ultrafine Pt NPs supported on N,S-codoped porous carbon nanofibers (Pt–N,S-pCNFs) hybrids were prepared by electrospinning, hydrothermal and calcination approaches. Notably, the ultrafine Pt NPs (about 4.0 nm) were first obtained through the dispersion and reduction of polyvinylpyrrolidone (PVP), and were further uniformly dispersed on pCNFs. The ultrafine and uniform dispersion of Pt NPs and N and S dopants could greatly improve oxygen adsorption, afford more active sites, and enhance electron mobility. Here, the Pt–N,S-pCNFs hybrids are used as electrocatalysts, and exhibit outstanding ORR properties and excellent long-term durability for HER and OER. Thus, they can be applied as highly efficient catalysts in hydrogen production by water splitting. In addition, Pt–N,S-pCNFs hybrids show a high hydrogen capacity, which suggests their ability to serve as hydrogen storage materials as well. Therefore, the convenient preparation, high N/S content and uniform dispersion of Pt NPs endow the Pt–N,S-pCNFs hybrids with superb ORR, OER and HER performance as well as high hydrogen adsorption capacity.

Results and discussion

The fabrication procedure to synthesize ultrafine Pt NPs supported on N,S-pCNFs is schematically illustrated in Fig. 1 and in the ESI.† PAN/PVP nanofibers were first obtained from electrospinning with a mixture of PAN/PVP/DMF solution. Under further hydrothermal treatment, PVP was removed from the PAN/PVP nanofibers and thiourea and H_2PtCl_6 were incorporated and then dried on the fibers. Subsequently, the mixture was preoxidized and carbonized at 220 °C and 900 °C under argon atmosphere to obtain the Pt–N,S-pCNFs hybrids.

The XRD patterns were recorded to validate the successful preparation of the ultrafine Pt–N,S-pCNFs hybrids. As shown in Fig. 2(a), the main peak at 25.3° is evident for pCNFs, N-pCNFs, N,S-pCNFs, and Pt–N,S-pCNFs, which is attributed to the graphite (002) crystalline plane with a hexagonal structure. Meanwhile, all Pt peaks located at 40.2°, 46.3°, 67.8° and 81.2° appear after the Pt NPs (JPDS#PDF#65-2868) were doped on N,S-pCNFs, which is consistent with the typical face-centered-cubic (111), (200), (220) and (311) crystalline planes from Pt NPs, respectively. These peaks are different from the diffraction patterns of the pCNFs, N-pCNFs and N,S-pCNFs hybrids. Furthermore, the Raman spectra of pCNFs, N-pCNFs, N,S-pCNFs, and Pt–N,S-pCNFs were investigated (Fig. 2(b)). All of the samples display two main Raman peaks located at around 1349 and 1583 cm^{-1}, which correspond to the disordered (D band) and graphitic carbons (G band), respectively.[60] The ID/IG band intensity ratio of Pt–N,S-pCNFs (1.02) is lower than that of pCNFs (1.31), N-pCNFs (1.20), and N,S-pCNFs (1.18), indicating the high graphitization of Pt–N,S-pCNFs. These results suggest that a large amount of N, S, and Pt atoms can be codoped into pCNFs. Such an enhanced graphitic structure would result in increased conductivity in Pt–N,S-pCNFs, which is beneficial to the ORR, OER, HER and hydrogen absorption processes.

The Pt–N,S-pCNFs hybrids show the morphology of ultrafine Pt NPs on N,S-pCNFs (a size of ~200 nm) according to the SEM results (Fig. 3(a)–(c)). The SEM images of pCNFs, N-pCNFs, and N,S-pCNFs are illustrated in Fig. S1.† The EDS spectrum (Fig. 3(d)) also indicates the presence of N, S, and Pt elements, further confirming the Pt decoration on the N, S codoped pCNFs. Meanwhile, the nitrogen adsorption/desorption isotherms of the Pt–N,S-pCNFs hybrids and the derived pore size distributions are plotted in Fig. 3(e). BET measurements exhibit a high specific surface area of 436.05 $m^2\ g^{-1}$. The corresponding pore size distribution (PSD) gradually narrows down to about 1.20 nm, which is calculated using the Barrett–Joyner–Halenda (BJH) method. The pCNFs possess a nanoporous structure, which offer abundant sites for atomically dispersed N and S, which act as coordination sites for Pt atoms in order to hinder ultrafine Pt NP migration and coalescence

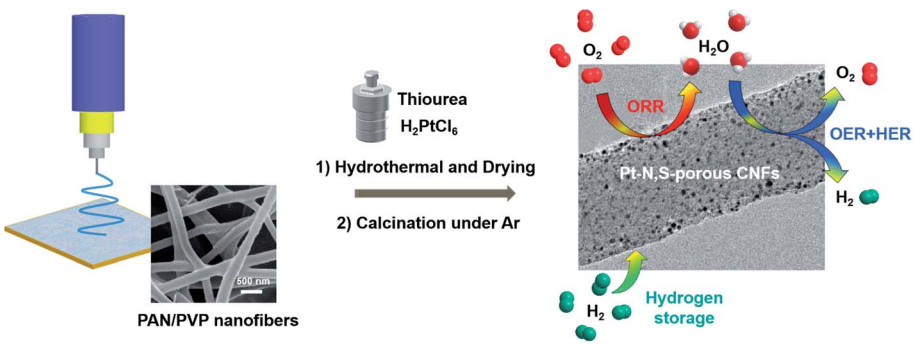

Fig. 1 Schematic illustration of the preparation process and application of the Pt–N,S-pCNFs hybrids.

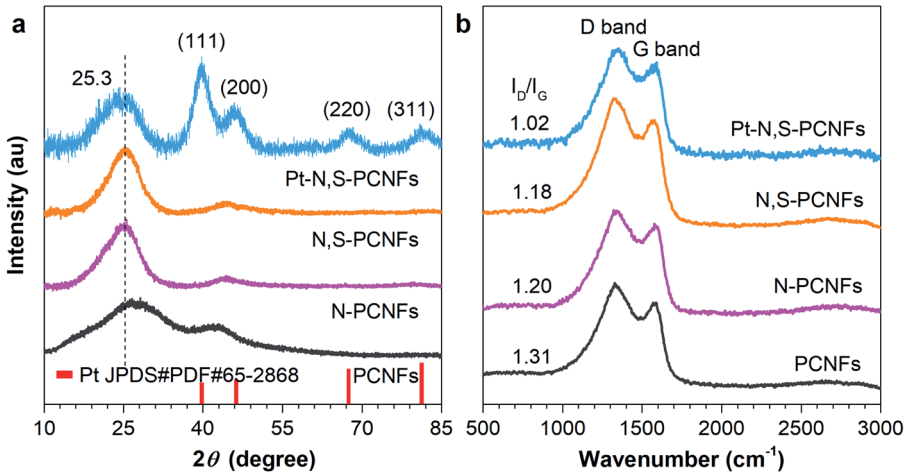

Fig. 2 (a) XRD and (b) Raman spectra of the pCNFs, N-pCNFs, N,S-pCNFs and Pt–N,S-pCNFs hybrids.

during electrocatalysis. Thus, the nanopores on pCNFs can contribute to the rapid transport of H_2O molecules, oxygen, and hydrogen gas, associated with enhancing the electrocatalytic features of the Pt–N,S-pCNFs hybrids.

To gain more insight from the morphology of the Pt–N,S-pCNFs hybrids, high-resolution transmission electron microscopy (HRTEM) was used (Fig. 4). The TEM measurements and the PSD of Pt–N,S-pCNFs at different magnifications show that the Pt NPs are round-shaped and uniformly dispersed in pCNFs, hence, there is no formation of Pt NP aggregates (Fig. 4(a)). As shown in the magnified TEM images (Fig. 4(b)), the corresponding PSD histograms are obtained by calculating the size of more than 150 randomly selected particles. For the Pt–N,S-pCNFs hybrids, the mean size diameter of Pt NPs is centered around 4.0 nm, and a narrow size distribution is obtained (Fig. 4(d)). Meanwhile, the HRTEM image clearly defines distinguishable lattice fringes, as highlighted by two white lines (spacing of 2.30 Å) (Fig. 4(c)). These are consistent with the face-centered cubic (fcc) (111) crystalline planes of Pt NPs,[61,62] indicating that Pt NPs are successfully deposited on N,S-pCNFs.

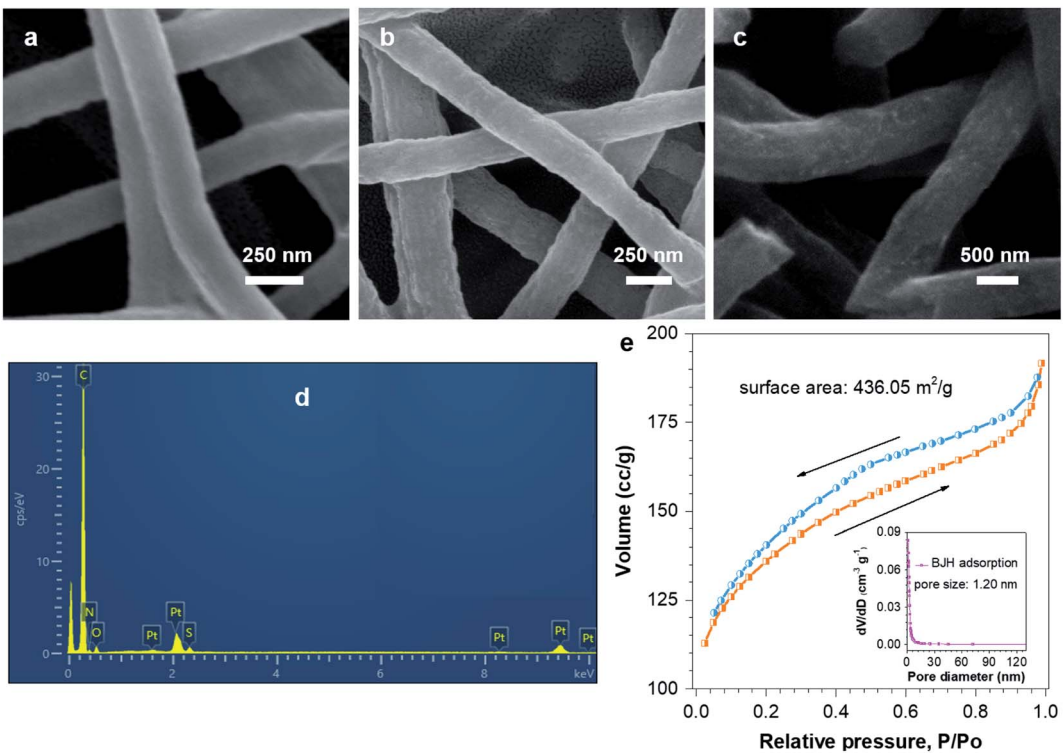

Fig. 3 SEM images of (a) PAN/PVP nanofibers, (b) H_2PtCl_6-thiourea porous PAN nanofibers and (c) Pt–N,S-pCNFs hybrids. (d) EDS spectrum and (e) N_2 adsorption–desorption isotherms of the Pt–N,S-pCNFs hybrids together with their PSD curve (inset).

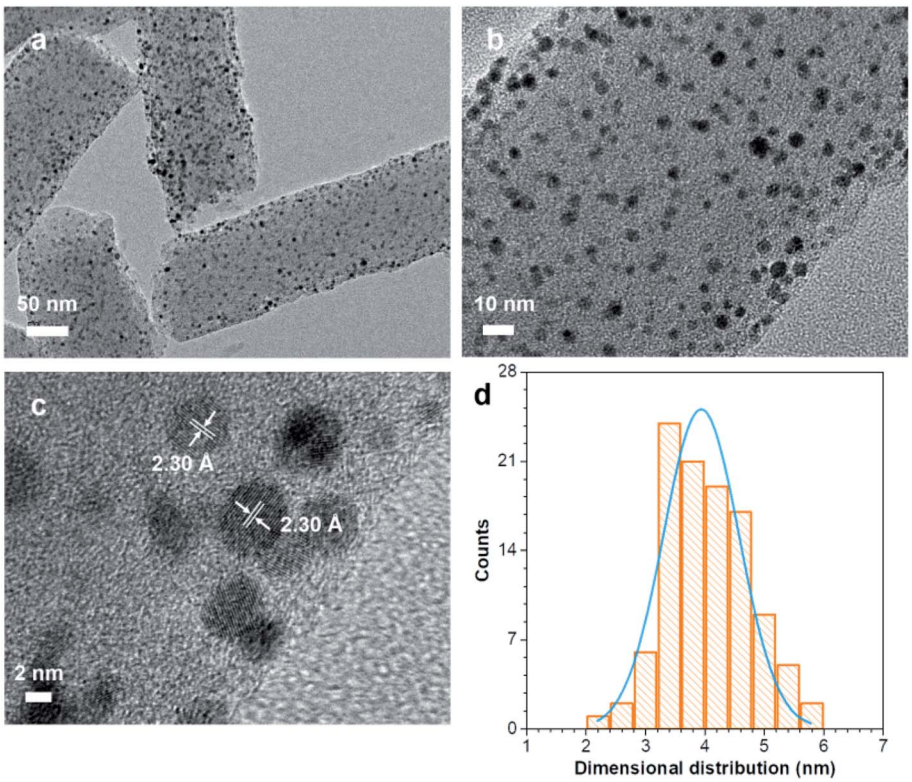

Fig. 4 (a)–(c) TEM images at different magnifications and (d) the particle size distribution of Pt NPs from Pt–N,S-pCNFs.

This contributes to the enhancement of the electrocatalytic properties towards ORR, OER, HER and hydrogen storage.

To obtain more information about the functionalities of the N, S and Pt atoms after the codoping and decorating processes, the XPS survey spectrum of the Pt–N,S-pCNFs hybrids was conducted. As shown in Fig. 5, C 1s, N 1s, S 2p, O 1s and Pt 4f peaks are present. The C, N, S, O and Pt contents remain at a high level up to *ca.* 78.25%, 8.83%, 1.72%, 9.37% and 1.82%, respectively, on the Pt–N,S-pCNFs hybrids. The C 1s spectrum of Pt–N,S-pCNFs is shown in Fig. 5(b), which can be divided into three regions. The sp^2-conjugated carbon network is confirmed by the high intensity of the C–C bond (284.6 eV). The C–O (286.0 eV) and C–N (285.7 eV) bonds in Pt–N,S-pCNFs are also detected. The N 1s spectrum in Fig. 5(c) can be deconvoluted into four regions: pyridinic-nitrogen (397.8 eV, 51.0%), pyrrolic-nitrogen (399.6 eV, 33.3%), graphitic-nitrogen (400.8 eV, 9.3%), and oxidized-nitrogen (402.5 eV, 6.4%).[63] Pyridinic-nitrogen and graphitic-nitrogen are predominant, contributing to the adsorption of oxygen and hydrogen gas. Meanwhile, it can be clearly seen from the S 2p deconvoluted peaks (Fig. 5(d)) that two configurations of sulfur are incorporated into pCNFs: thiophene (S–C–S) (162.5 eV) and oxidized (SOx-C) (163.9 eV) sulfur species. Compared to pure pCNFs, the higher nitrogen and sulfur concentration of Pt–N,S-pCNFs offers better ORR, OER, HER and hydrogen adsorption density.[64]

As seen in the spectrum of Pt 4f, which can be deconvoluted into two pairs of doublets (Fig. 5(e)), the peak binding energies of Pt $4f_{7/2}$ and $4f_{5/2}$ at 70.3 eV and 73.8 eV, respectively, coincide with the sharp doublet, which is close to the values of metallic Pt (0). The two doublets at 71.2 eV and 74.5 eV are attributed to Pt(II) species such as platinum oxide (PtO)[65] resulting from the slight oxidation of Pt NPs by exposure to air. As seen in the spectrum of Pt 4f, the Pt species in the Pt–N,S-pCNFs hybrids are metallic Pt (0) (41.9%) and PtO (58.1%), respectively. While the peak at 529.83 eV corresponds to the oxygen species, those at 531.09 eV and 532.31 eV are attributed to the residual oxygen-containing groups (for example –OH and –COOH) on the surface of Pt–N,S-pCNFs (Fig. 5(f)). The XPS analysis results demonstrate that the Pt–N,S-pCNFs hybrids are successfully prepared and the reason for their enhanced catalytic activity is revealed to be the existence of elemental valence states.

Oxygen reduction reaction

To comprehensively evaluate the ORR catalytic activity of the pCNFs, N-pCNFs, N,S-pCNFs, and Pt–N,S-pCNFs catalysts, cyclic voltammograms (CV) and measurements on a rotating disk electrode (RDE) were conducted, and Fig. 6(a) exhibits the detailed results. From the CV spectra, it can be seen that there are strong and intense cathodic peaks with a higher current density in the O_2-saturated electrolyte as compared with that in the N_2-saturated electrolyte.

The above-mentioned results suggest that Pt–N,S-pCNFs possesses a good electrocatalytic activity towards ORR. The ORR activity comparison for pCNFs, N-pCNFs, N,S-pCNFs, and Pt–N,S-pCNFs is summarized in Table 1. Evidently, pCNFs, N-

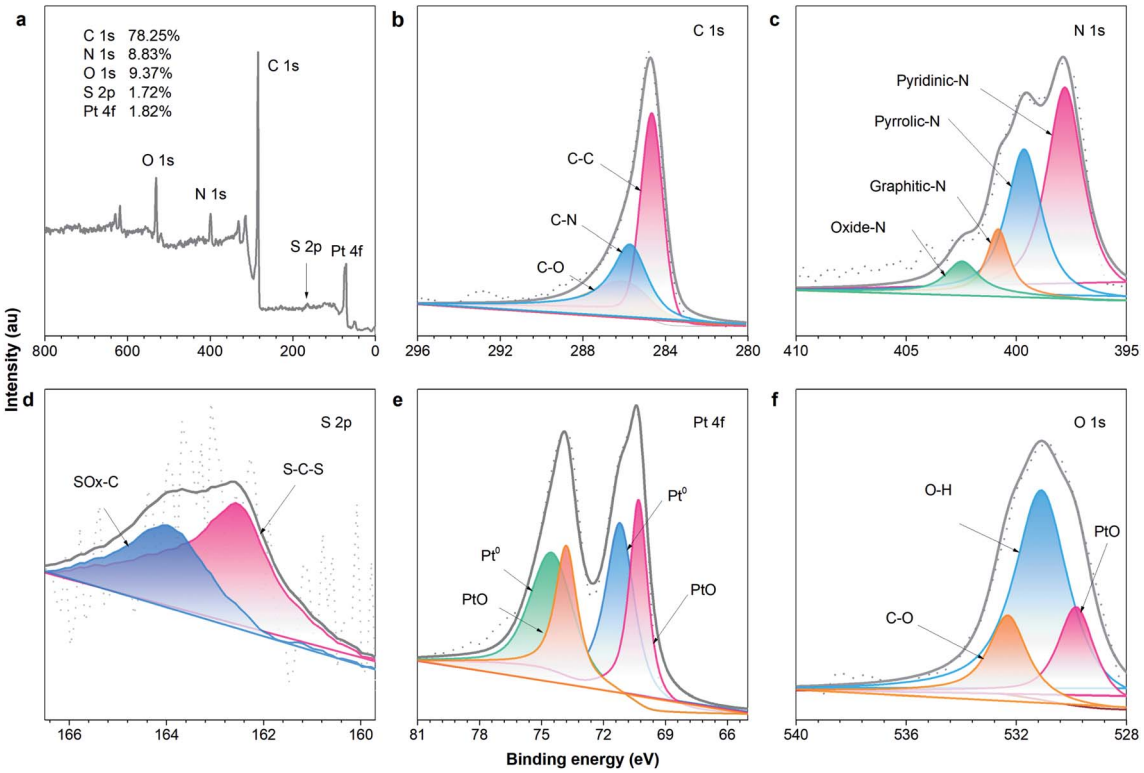

Fig. 5 XPS spectra of the (a) survey scan, (b) C 1s region, (c) N 1s region, (d) S 2p region, (e) Pt 4f region and (f) O 1s region of the Pt–N,S-pCNFs hybrids.

pCNFs, and N,S-pCNFs exhibit remarkable electrocatalytic ORR activity, associated with the onset potential (0.83, 0.86 and 0.88 V *vs.* RHE) being close to that of Pt/C-20 wt% (0.95 V), which is indicated by the synergistic ORR catalytic activity of nitrogen, sulfur and Pt NPs in the hybrids.[66,67] Compared with Pt–N-pCNFs (0.91 V) (Fig. S2†), the onset potential of Pt–N,S-pCNFs is substantially more positive (+1.02 V), and is among the best reported by far.[68–70] Such a positive shift of up to 70 mV signifies the remarkably enhanced electrocatalytic performance of Pt–N,S-pCNFs in the oxygen reduction reaction compared with that of Pt/C-20 wt%, which is due to the electronic interactions among the Pt NPs, nitrogen and sulfur dopants, and pCNFs. The interaction of the nitrogen and sulfur dopants could lead to an increase in the spin and charge density of the atoms present in the CNFs to enhance oxygen adsorption and ORR activity.

To further assess the reaction kinetics of the pCNFs, N-pCNFs, N,S-pCNFs, Pt–N-pCNFs and Pt–N,S-pCNFs hybrids, LSVs were then recorded using a RDE with a scan rate of 10 mV s^{-1} in an O_2-saturated alkali electrolyte (Fig. 6(b), S3(a),† 4(a) and 5(a)). Among the prepared freestanding catalysts, the half-wave potentials ($E_{1/2}$) at 1600 rpm of the pCNFs, N-pCNFs, N,S-pCNFs, Pt–N-pCNFs and Pt–N,S-pCNFs hybrids are 0.65, 0.63, 0.71, 0.77 and 0.83 V, respectively, close to that of Pt/C-20 wt% (0.83 V), due to the effectively increased basal spacing and electrical conductivity, which resulted from the synergistic effects and the interpenetrated network structure of the combination of N, S and Pt NPs with pCNFs.

Moreover, the RDE curves of pCNFs, N-pCNFs, N,S-pCNFs, Pt–N-pCNFs and Pt–N,S-pCNFs were also measured to determine their ORR kinetic performance in alkaline electrolyte at various rotation speeds (Fig. 6(c)).[71] The linearity and parallelism of the K–L plots suggest reaction kinetics of ORR towards the concentration of dissolved oxygen and the n at different potentials (Fig. 6(d), S3(b),† 4(b), 5(b)). The n of pCNFs, N-pCNFs, N,S-pCNFs, Pt–N-pCNFs and Pt–N,S-pCNFs at 0.6 V are calculated to be 2.4, 3.6, 3.1, 2.6 and 4.2, respectively, from the slopes of the K–L plots (Fig. 6(e) and S3–S5†), indicating that the Pt–N,S-pCNFs hybrids favor the 4e oxygen reduction process in alkaline electrolyte.[72] The electrochemical impedance spectra (EIS) of Pt–N-pCNFs and Pt–N,S-pCNFs are measured (Fig. S6†). The low resistances of Pt–N-pCNFs (79.36 Ω) and Pt–N,S-pCNFs (71.85 Ω) indicate their better charge conductivity, which may arise from heteroatom-doping induced charge transfer in carbon and the high electrical conductivity of Pt.

In addition, the ORR catalytic activity of Pt–N,S-pCNFs in acidic solution was measured. The onset potential, half-wave potentials, limit currency density and n of Pt–N,S-pCNFs are 0.76 V, 0.64 V, 5.4 mA cm^{-2} and ~4 (Fig. S7†), respectively. Therefore, Pt–N,S-pCNFs exhibit better ORR performance in acidic electrolyte.

The long-term durability of catalysts is also a major concern in fuel cell technology. The durability of the N,S-pCNFs, Pt–N,S-pCNFs and Pt/C-20 wt% catalysts were obtained at a constant voltage of 0.62 V (*vs.* RHE) for 10 000 s in O_2-saturated alkaline electrolyte (Fig. 6(f)). The chronoamperometric response of Pt–

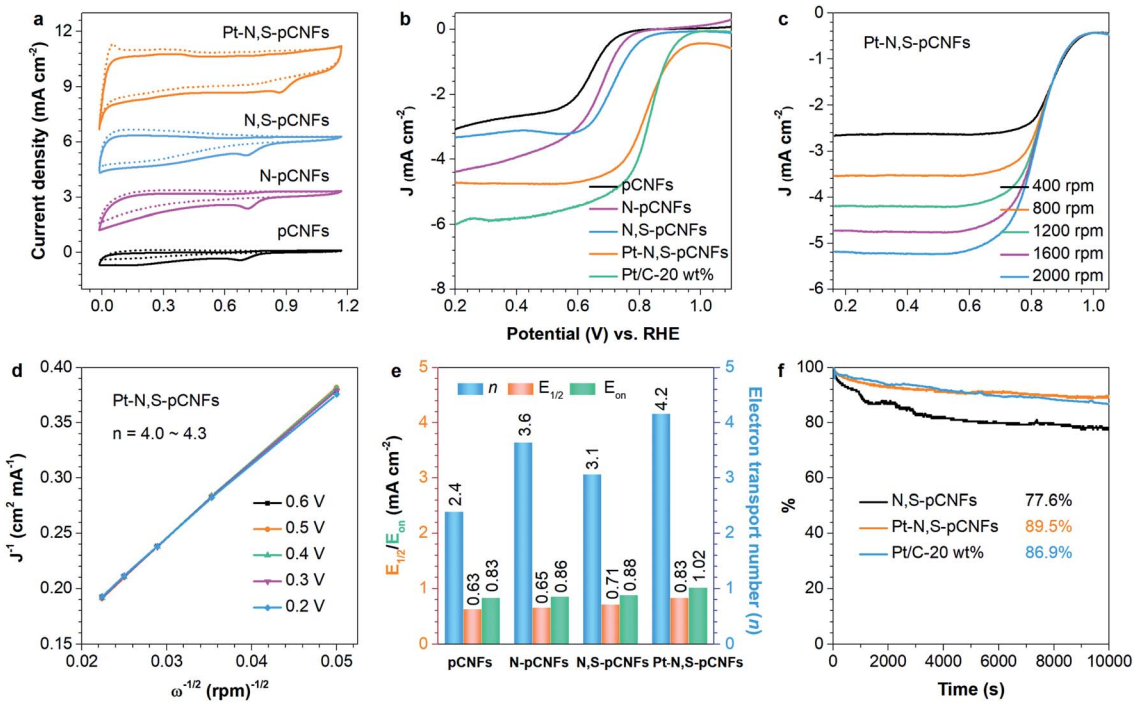

Fig. 6 (a) CV curves of pCNFs, N-pCNFs, N,S-pCNFs, and Pt–N,S-pCNFs on glassy carbon electrodes in N_2-(dotted line) and O_2-saturated (solid line) electrolyte with a scan rate of 10 mV s^{-1}. (b) Linear sweep voltammograms (LSVs) for pCNFs, N-pCNFs, N,S-pCNFs, Pt–N,S-pCNFs and Pt/C-20 wt% at 1600 rpm. (c) LSV curves of Pt–N,S-pCNFs at different rotation rates (in rpm). (d) The corresponding Koutecky–Levich (K–L) plot of Pt–N,S-pCNFs obtained from the RDE curves at 0.2–0.6 V with *n*. (e) Eon, $E_{1/2}$ and *n* of pCNFs, N-pCNFs, N,S-pCNFs, and Pt–N,S-pCNFs. (f) Chronoamperometric response of N,S-pCNFs, Pt–N,S-pCNFs and Pt/C-20 wt% modified glassy carbon (GC) electrodes at 0.62 V and 1600 rpm. The electrolyte solution is 0.1 M KOH.

N,S-pCNFs retains a higher relative current with 89.5% in the alkaline electrolyte, compared with that of Pt/C-20 wt% (86.9%) and Pt–N-pCNFs (64.1%). The better long-term durability of Pt–N,S-pCNFs could be attributed to the outstanding confined structure of Pt and N, S codoping into the pCNFs, which enhances their interfacial contact, inhibits the dissolution/agglomeration of Pt NPs, and promotes the transfer of electrolyte ions.[73]

Water-splitting measurements

The OER and HER performances of Pt–N-pCNFs, Pt–N,S-pCNFs and IrO_2 were tested in alkaline electrolyte with a scan rate of 10 mV s^{-1}. The OER and HER polarization curves of Pt–N,S-pCNFs and IrO_2 (Fig. 7(a) and (b), S8, S9†) show lower overpotentials of 450 mV and 168 mV with 10 mA cm^{-2} compared with that of Pt–N-pCNFs (499 mV and 212 mV), indicating the high OER and HER activity of Pt–N,S-pCNFs. To characterize the stability of Pt–N,S-pCNFs in OER and HER, CV scanning of Pt–N,S-pCNFs was performed for 1000 cycles. Its polarization curves almost coincide with the initial curves, with worse performance than IrO_2 but better than that of Pt–N-pCNFs. The Tafel curves of IrO_2, Pt–N-pCNFs and Pt–N,S-pCNFs were also calculated. From the slope of the corresponding Tafel curve (Fig. S10 and S11†), the Tafel slope of Pt–N,S-pCNFs is 220 mV dec^{-1}, which is lower than that of IrO_2 (180 mV dec^{-1}) but higher than that of Pt–N-pCNFs (230 mV dec^{-1}). The results further indicate the excellent HER activity of Pt–N,S-pCNFs due to the synergistic effect of the doping of nitrogen and sulfur and platinum loaded on pCNFs.[74]

Moreover, the performance of water splitting for Pt–N,S-pCNFs was studied in alkaline electrolyte, as shown in Fig. 7(c), where the polarization curve exhibits good catalytic

Table 1 The ORR electrocatalytic activity comparison for the pCNFs, N-pCNFs, N,S-pCNFs, Pt–N-pCNFs, Pt–N,S-pCNFs and Pt/C-20 wt% hybrids

	pCNFs	N-pCNFs	N,S-pCNFs	Pt–N-pCNFs	Pt–N,S-pCNFs	Pt/C-20 wt%
E_{onset} [a] (V *vs.* RHE)	0.83	0.86	0.88	0.91	**1.02**	0.95
$E_{1/2}$ [b] (V *vs.* RHE)	0.63	0.65	0.71	0.77	**0.83**	0.83
n [c]	2.4	3.6	3.1	2.6	**4.2**	4

[a] E_{onset} = onset potential. [b] $E_{1/2}$ = half-wave potential. [c] n = electron transport number.

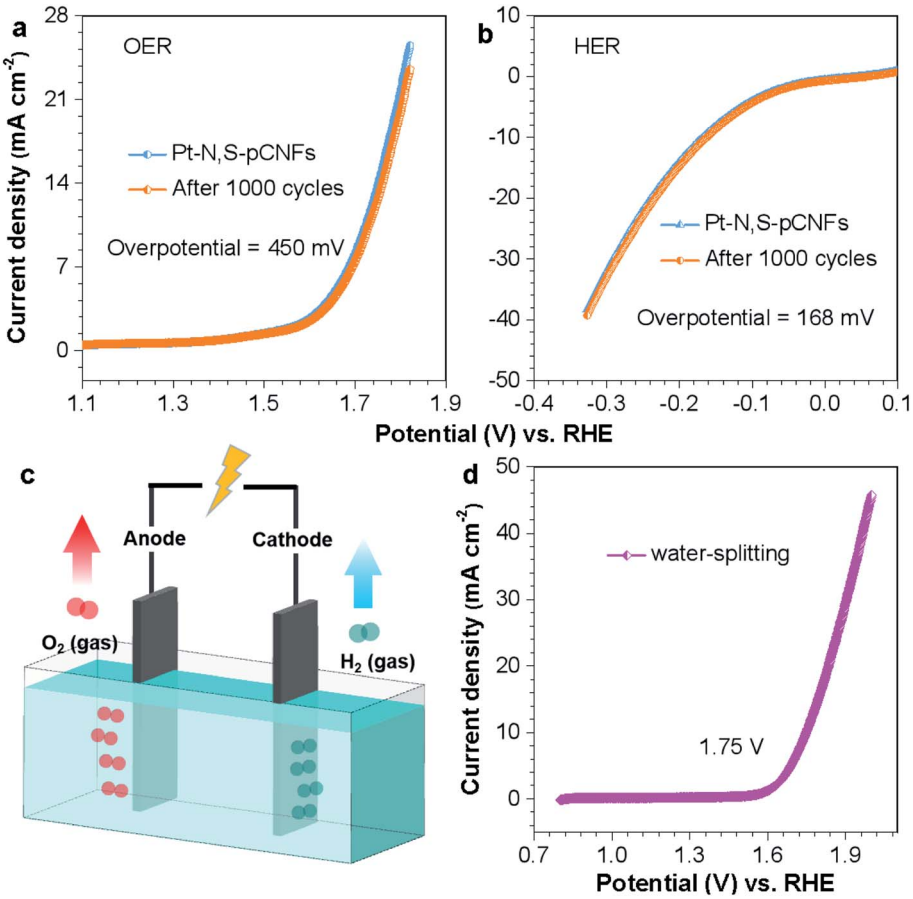

Fig. 7 (a) OER and (b) HER LSV curves recorded for Pt–N,S-pCNFs before and after 1000 cycles. (c) Schematic diagram of an electrolyzer for water splitting. (d) Polarization curves of Pt–N,S-pCNFs for overall water splitting. The alkaline electrolyte = 1 M KOH solution.

performance and shows a current density of 10 mA cm^{-2} at 1.75 V (Fig. 7(d)). This is derived from the unique synergistic effect of the N, S heteroatom codoping and ultrafine Pt NPs.

Hydrogen adsorption measurements

The hydrogen adsorption experiments of pCNFs, N-pCNFs, N,S-pCNFs and Pt–N,S-pCNFs were performed at 10 MPa, 20 °C. Fig. 8 exhibits typical high-pressure hydrogen adsorption isotherms, which show that the increasing hydrogen concentration is dependent on the extension of adsorption time. The adsorption performances of the pCNFs, N-pCNFs and N,S-pCNFs hybrids are completed within 7200 s, and their storage capacities are 0.04, 0.20 and 0.69 wt%, respectively. These results illustrate that N,S-pCNFs can increase hydrogen adsorption due to the nitrogen and sulfur doped in pCNFs.

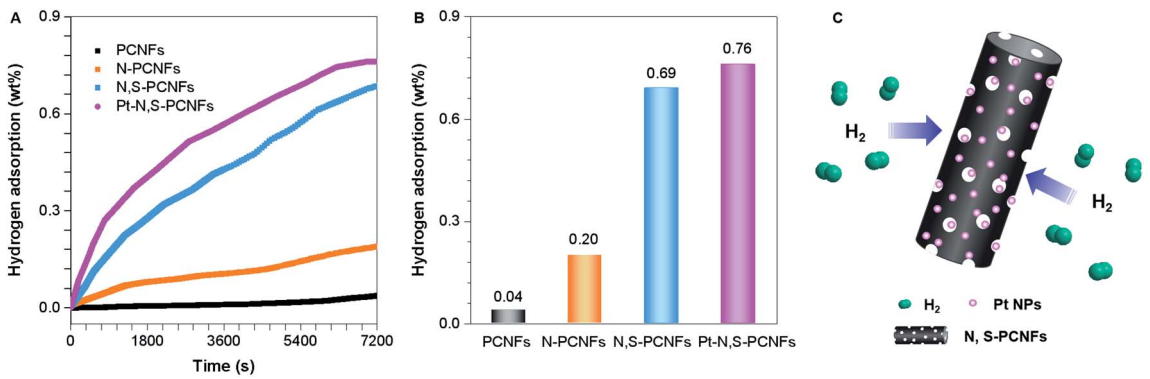

Fig. 8 (a) Hydrogen adsorption spectra and (b) capacity of the pCNFs, N-pCNFs, N,S-pCNFs, and Pt–N,S-pCNFs hybrids at 20 °C and 10 MPa. (c) The schematic diagram of hydrogen adsorption for the Pt–N,S-pCNFs hybrids.

To further enhance the hydrogen storage capacity, ultrafine Pt NPs are introduced and uniformly dispersed on the surface of N,S-pCNFs. The hydrogen storage capacity of Pt–N,S-pCNFs is about 0.76 wt% under the same conditions (Fig. 8(b)), which is enhanced due to the increased content of N, S and Pt dopants. This is due to the high electron affinity of the sp^2 carbon framework codoped with N and S atoms, which can provide strong stabilization between Pt–N,S-pCNFs and H_2 (Fig. 8(c)). Moreover, nano-sized pores (1.20 nm) of the Pt–N,S-pCNFs hybrid results in the capillary condensation of hydrogen gas, which improves the hydrogen storage performance.[75] Thus, these results suggest that N and S codoping in the Pt–N,S-pCNFs hybrids can enhance the adsorption energy of hydrogen atoms at neighboring C-atom sites and the Pt NPs can increase the ability of hydrogen storage *via* the spillover effect.

Conclusions

In summary, we report a novel and simple preparation method for Pt–N,S-pCNFs hybrids with remarkable performance in ORR, OER, HER and hydrogen storage. The ultrafine Pt NPs supported on N,S-pCNFs were synthesized by facile electrospinning, hydrothermal treatment and carbonization. Impressively, PVP acts not only as a reducing agent in the preparation of Pt NPs but also as a dispersant to prevent the agglomeration of Pt NPs. The porous carbon framework also greatly supplements the Pt NPs with even distribution, effective space confinement and large specific surface area (436.05 m^2 g^{-1}). These results indicate the excellent electrocatalytic activity of Pt–N,S-pCNFs for ORR, OER, and HER in alkaline electrolytes, with advantages such as a high electron transfer number (4.2), high onset potential (1.02 eV), large $E_{1/2}$ (0.83 eV) and superior durability (89.5%) for ORR and good long-term durability for OER and HER. Pt–N,S-pCNFs can also be used as a highly efficient electrocatalyst for water splitting, which shows a current density of 10 mA cm^{-2} at 1.75 V. The Pt–N,S-pCNFs hybrid also demonstrates a high hydrogen storage capacity of 0.76 wt% under 10 MPa, 20 °C. Therefore, the synthetic strategy of the hybrids provides a simplified and feasible route for the direct fabrication of efficient multifunctional electrocatalysts and could be further extended to the development of other transition metals or metal oxide/carbon-supported materials for a variety of applications, such as lithium–air batteries, supercapacitors and others.

Author contributions

This work was completed through the contribution of all authors. The preparation of Pt–N,S-pCNFs used in this work and most of the electrochemical property tests were conducted by Xiaohong Chen, Kai Niu, Xundao Liu and Bao Zhang. With the help of Zhiyong Xue, Bogu Liu, Hong Zeng, and Wei Lv, the fitting lines of XRD and XPS were successfully completed. Prof. Yongming Zhang and Prof. Ying Wu directed the whole process and revised the manuscript. All authors have given their approval to the final version of this manuscript.

Conflicts of interest

There are no conflicts to declare.

Acknowledgements

This work was financially supported by the National Key Research and Development Plan (Grant No. 2018YFB1502102), the Postdoctoral Innovative Talent Support Program of China (Grant No. BX20190112), the National Natural Science Foundation of China (Grant No. 52071141, 51971092, 51771056, 51803073), Interdisciplinary Innovation Program of North China Electric Power University (grant number XM2112355), and the Fundamental Research Funds for the Central Universities (Grant No. 2021MS051). The authors express their appreciation for Ms Shengnan Kong at the Instrumental Analysis Center of Shanghai Jiao Tong University.

References

1 Y. Xiong, M. You, F. Liu, M. Wu, C. Cai, L. Ding, C. Zhou, M. Hu, W. Deng and S. Wang, *ACS Appl. Energy Mater.*, 2020, **3**, 2490.
2 Q. Liu, L. Du, G. Fu, Z. Cui, Y. Li, D. Dang, X. Gao, Q. Zheng and J. B. Goodenough, *Adv. Energy Mater.*, 2019, **9**, 1803040.
3 Q. Liu, Q. Kang, Z. Wang, Q. Lu and F. Gao, *Dalton Trans.*, 2021, **50**, 6297.
4 Q. Wang, L. Zhang, Y. Liu, G. Zhang and P. Zhu, *Carbohydr. Polym.*, 2020, **232**, 115693.
5 L. Zu, W. Zhang, L. Qu, L. Liu, W. Li, A. Yu and D. Zhao, *Adv. Energy Mater.*, 2020, 2002152.
6 J. Hu, R. Li, S. Zhu, G. Zhang and P. Zhu, *Cellulose*, 2021, **28**, 4991.
7 Y. Chen, T. Cheng and W. A. Goddard III, *J. Am. Chem. Soc.*, 2020, **142**, 8625.
8 F. Zheng, Y. Fan and W. Chen, *ACS Appl. Mater. Interfaces*, 2021, **13**, 38170.
9 Z. Zhuang, C. Du, P. Li, Z. Zhang, Z. Fang, J. Guo and W. Chen, *Electrochim. Acta*, 2021, **368**, 137608.
10 J. Yan, Y. Wang, Y. Zhang, S. Xia, J. Yu and B. Ding, *Adv. Mater.*, 2020, 2007525.
11 H. Su, S. Zhou, X. Zhang, H. Sun, H. Zhang, Y. Xiao, K. Yu, Z. Dong, X. Dai and X. Huang, *Dalton Trans.*, 2018, **47**, 16567.
12 C. Ji, G. Yang, P. R. Ilango, J. Song, D. Yu, S. Han, D. Zhang, L. Li and S. Peng, *Chem.–Asian J.*, 2020, **15**, 19572.
13 Z. Zhang, Q. Dong, P. Li, S. L. Fereja, J. Guo, Z. Fang, X. Zhang, K. Liu, Z. Chen and W. Chen, *J. Phys. Chem. C*, 2021, **125**, 24814.
14 S. L. Fereja, P. Li, J. Guo, Z. Fang, Z. Zhang, Z. Zhuang, X. Zhang, K. Liu and W. Chen, *ACS Appl. Nano Mater.*, 2021, **4**, 5992.
15 J. Liu, M. Jiao, B. Mei, Y. Tong, Y. Li, M. Ruan, P. Song, G. Sun, L. Jiang, Y. Wang, Z. Jiang, L. Gu, Z. Zhou and W. Xu, *Angew. Chem., Int. Ed.*, 2019, **58**, 1163.
16 S. M. Alia, G. Zhang, D. Kisailus, D. Li, S. Gu, K. Jensen and Y. Yan, *Adv. Funct. Mater.*, 2010, **20**, 37426.

17 X.-K. Wan, G. Samjeské, H. Matsui, C. Chen, S. Muratsugu and M. Tada, *Dalton Trans.*, 2021, **50**, 6811.
18 S. Shao, Y. Xiao, J. Yang, X. Lv, K. Feng, Y. Xia, D. Zhang, H. Xu, J. Zhong and J. Deng, *Chem. Eng. J.*, 2021, **413**, 127416.
19 X. Zhou, X. Liu, J. Zhang, C. Zhang, S. J. Yoo, J.-G. Kim, X. Chu, C. Song, P. Wang, Z. Zhao, D. Li, W. Zhang and W. Zheng, *Carbon*, 2020, **166**, 284.
20 Y. Tong and P. Chen, *Dalton Trans.*, 2021, **50**, 7776.
21 S. Shanmugapriya, P. Zhu, C. Yan, A. M. Asiri, X. Zhang and R. K. Selvan, *Adv. Mater. Interfaces*, 2019, **6**, 1900565.
22 M. Nadeem, G. Yasin, M. Arif, H. Tabassum, M. H. Bhatti, M. Mehmood, U. Yunus, R. Iqbal, T. A. Nguyen, Y. Slimani, H. Song and W. Zhao, *Chem. Eng. J.*, 2021, **409**, 128205.
23 J.-Q. Chi, J.-Y. Xie, W.-W. Zhang, B. Dong, J.-F. Qin, X.-Y. Zhang, J.-H. Lin, Y.-M. Chai and C.-G. Liu, *ACS Appl. Mater. Interfaces*, 2019, **11**, 4047.
24 G. M. Psofogiannakis and G. E. Froudakis, *J. Phys. Chem. C*, 2009, **113**, 14908.
25 Y. Li and R. T. Yang, *J. Phys. Chem. C*, 2007, **111**, 11086.
26 N. R. Stuckert, L. Wang and R. T. Yang, *Langmuir*, 2010, **26**, 11963.
27 Z. Wang and R. T. Yang, *J. Phys. Chem. C*, 2010, **114**, 5956.
28 C.-S. Tsao, Y.-R. Tzeng, M.-S. Yu, C.-Y. Wang, H.-H. Tseng, T.-Y. Chung, H.-C. Wu, T. Yamamoto, K. Kaneko and S. Chen, *J. Phys. Chem. Lett.*, 2010, **1**, 1060.
29 C.-S. Tsao, Y. Liu, M. Li, Y. Zhang, J. B. Leao, H.-W. Chang, M.-S. Yu and S.-H. Chen, *J. Phys. Chem. Lett.*, 2010, **1**, 1569.
30 H. Meng, X. Chen, T. Gong, H. Liu, Y. Liu, H. Li and Y. Zhang, *ChemCatChem*, 2019, **11**, 6015.
31 Y. Xiong, M. You, F. Liu, M. Wu, C. Cai, L. Ding, C. Zhou, M. Hu, W. Deng and S. Wang, *ACS Appl. Energy Mater.*, 2020, **3**, 2490.
32 S. Pei, Z. Zhou, X. Chen, X. Huang, T. Liu, B. Cao and F. Wang, *Int. J. Electrochem. Sci.*, 2016, **11**, 8994.
33 X. Chen, Z. Ning, Z. Zhou, X. Liu, J. Lei, S. Pei and Y. Zhang, *RSC Adv.*, 2018, **8**, 27246.
34 H. Meng, Y. Liu, H. Liu, S. Pei, X. Yuan, H. Li and Y. Zhang, *ACS Appl. Mater. Interfaces*, 2020, **12**, 41580.
35 S. Chao, Q. Xia, Y. Wang, W. Li and W. Chen, *Dalton Trans.*, 2020, **49**, 433.
36 X. Liu, D. Wu, X. Liu, X. Luo, Y. Liu, Q. Zhao, J. Li and D. Dong, *Electrochim. Acta*, 2020, **336**, 135757.
37 Z. Fan, J. Yan, L. Zhi, Q. Zhang, T. Wei, J. Feng, M. Zhang, W. Qian and F. Wei, *Adv. Mater.*, 2010, **22**, 3723.
38 D. Kim, G. Kim, S. Oh, J. Park, S. Lee, S. Yoon, J. Lee, W. Lee, T.-Y. Jeon, E. Cho, K. Sohn, D.-K. Yang and J. Kim, *ACS Sustainable Chem. Eng.*, 2020, **8**, 8537.
39 M. Kaukonen, A. V. Krasheninnikov, E. Kauppinen and R. M. Nieminen, *ACS Catal.*, 2013, **3**, 159.
40 K. Ichihashi, S. Muratsugu, S. Miyamoto, K. Sakamoto, N. Ishiguro and M. Tada, *Dalton Trans.*, 2019, **48**, 7130.
41 S. Chen, Z. Wei, X. Qi, L. Dong, Y.-G. Guo, L. Wan, Z. Shao and L. Li, *J. Am. Chem. Soc.*, 2012, **134**, 13252.
42 L. Li, L. P. Hu, J. Li and Z. D. Wei, *Nano Res.*, 2015, **8**, 418.
43 S. M. Jayawickrama, Z. Y. Han, S. Kido, N. Nakashima and T. Fujigaya, *Electrochim. Acta*, 2019, **312**, 349.
44 Z. Yang, J. Li, Y. Ling, Q. Zhang, X. Yu and W. Cai, *ChemCatChem*, 2017, **9**, 3307.
45 M. Kato, R. Nakahoshiba, K. Ogura, S. Tokuda, S. Yasuda, K. Higashi, T. Uruga, Y. Uemura and I. Yagi, *ACS Appl. Energy Mater.*, 2020, **3**, 6768.
46 C. Wang, H. Gao, X. Chen, W. Z. Yuan and Y. Zhang, *Electrochim. Acta*, 2015, **152**, 383.
47 G. He, Y. Song, K. Liu, A. Walter, S. Chen and S. Chen, *ACS Catal.*, 2013, **3**, 831.
48 L. Wang, N. R. Stuckert, H. Chen and R. T. Yang, *J. Phys. Chem. C*, 2011, **115**, 4793.
49 C.-S. Tsao, Y.-R. Tzeng, M.-S. Yu, C.-Y. Wang, H.-H. Tseng, T.-Y. Chung, H.-C. Wu, T. Yamamoto, K. Kaneko and S.-H. Chen, *J. Phys. Chem. Lett.*, 2010, **1**, 1060.
50 L. Wan and R. T. Yang, *J. Phys. Chem. C*, 2009, **113**, 21883.
51 L. Wang, N. R. Stuckert, H. Chen and R. T. Yang, *J. Phys. Chem. C*, 2011, **115**, 4793.
52 G. M. Psofogiannakis and G. E. Froudakis, *J. Am. Chem. Soc.*, 2009, **131**, 15133.
53 A. Nikitin, X. Li, Z. Zhang, H. Ogasawara, H. Dai and A. Nilsson, *Nano Lett.*, 2008, **8**, 162.
54 H. Cheng, G. P. Pez and A. C. Cooper, *J. Am. Chem. Soc.*, 2001, **123**, 5845.
55 X. Chen, Z. Xue, K. Niu, X. Liu, W. lv, B. Zhang, Z. Li, H. Zeng, Y. Ren, Y. Wu and Y. Zhang, *RSC Adv.*, 2021, **11**, 4053.
56 B. Zhang, J. Yuan and Y. Wu, *Int. J. Hydrogen Energy*, 2019, **44**, 19294.
57 B. Zhang and Y. Wu, *Prog. Nat. Sci.: Mater. Int.*, 2017, **27**, 1127.
58 B. Liu, B. Zhang, Y. Wu, W. Lv and S. Zhou, *Int. J. Hydrogen Energy*, 2019, **44**, 27885.
59 C.-C. Huang, N.-W. Pu, C.-A. Wang, J.-C. Huang, Y. Sung and M.-D. Ger, *Sep. Purif. Technol.*, 2011, **82**, 210.
60 G. Zhang, Y. Xu, X. Xiang, G. Zheng, X. Zeng, Z. Li, T. Ren and Y. Zhang, *Tribol. Int.*, 2018, **126**, 39.
61 J. Chen, Q. Niu, G. Chen, J. Nie and G. Ma, *J. Phys. Chem. C*, 2017, **121**, 1463.
62 J. Kim, S. W. Lee, C. Carlton and Y. S. Horn, *J. Phys. Chem. Lett.*, 2011, **2**, 1332.
63 X. Liu, X. Luo, X. Chen, S. Zou, X. Liu, J. Li, H. Li and D. Dong, *J. Electroanal. Chem.*, 2020, **871**, 114283.
64 M. Chen, T. Le, Y. Zhou, F. Kang and Y. Yang, *ACS Appl. Energy Mater.*, 2020, **3**, 1653.
65 J. Melke, B. Peter, A. Habereder, J. Ziegler, C. Fasel, A. Nefedov, H. Sezen, C. Woll, H. Ehrenberg and C. Roth, *ACS Appl. Mater. Interfaces*, 2016, **8**, 82.
66 F. Chang, Z. Bai, M. Li, M. Ren, T. Liu, L. Yang, C.-J. Zhong and J. Lu, *Nano Lett.*, 2020, **20**, 2416.
67 Y. Li, L. Tang and J. Li, *Electrochem. Commun.*, 2009, **11**, 846.
68 D. P. He, K. Cheng, T. Peng, X. L. Sun, M. Pan and S. C. Mu, *J. Mater. Chem.*, 2012, **22**, 21298.
69 B. P. Vinayan, R. Nagar and S. J. Ramaprabhu, *J. Mater. Chem.*, 2012, **22**, 25325.
70 Y. M. Tan, C. F. Xu, G. X. Chen, N. F. Zheng and Q. J. Xie, *Energy Environ. Sci.*, 2012, **5**, 6923.
71 Z. Wang, R. Jia, J. Zheng, J. Zhao, L. Li, J. Song and Z. Zhu, *ACS Nano*, 2011, **5**, 1677.

72 K. Yamamoto, T. Imaoka, W. J. Chun, O. Enoki, H. Katoh, M. Takenaga and A. Sonoi, *Nat. Chem.*, 2009, **1**, 397.
73 V. Perazzolo, R. Brandiele, C. Durante, M. Zerbetto, V. Causin, G. A. Rizzi, I. Cerri, G. Granozzi and A. Gennaro, *ACS Catal.*, 2018, **8**, 1122.
74 P. Li, Z. Zhuang, C. Du, D. Xiang, F. Zheng, Z. Zhang, Z. Fang, J. Guo, S. Zhu and W. Chen, *ACS Appl. Mater. Interfaces*, 2020, **12**, 40194.
75 J. S. Im, S.-J. Park and Y.-S. Lee, *Int. J. Hydrogen Energy*, 2009, **34**, 1423.